A method to reduce the influence of ice-rafted debris on a grain size record from northern Fram Strait, Arctic Ocean

H. Christian Hass

The granulometric composition of terrigenous deep-sea sediments provides information on current speed if certain frame conditions are fulfilled. These include that current transport is the only transport process. At high latitudes this type of investigation is impaired due to the influence of ice-rafted debris (IRD) which contaminates the current-sorted grain size fractions. This study presents a new method that addresses this problem by setting the ice-rafted sand in relation to the silt of both current- and ice-transported origin. Deviations from the resulting regression function are then used to determine the behaviour of the silt mean grain size as a function of current speed largely independent from IRD bias. The study is based on sediments from the Yermak Plateau, Arctic Ocean, a region influenced by IRD brought with the south-headed Transpolar Drift and by north-directed bottom currents. The IRD correction results in displaying changes of current speed at much higher clarity; climate forcing of the currents becomes more evident. For example, the 8200 year cold event shows up as a major event in the corrected record whereas it is hardly visible in the original record.

H. C. Hass, Alfred Wegener Institute for Polar and Marine Research, Wadden Sea Research Station, Hafenstrasse 43, D-25992 List/Sylt, Germany.

The global ocean circulation system called the Ocean Conveyor forms the most powerful climate engine on Earth. It plays a crucial role in storing and distributing heat on a global scale (Broecker 1991). On their way north from the tropic latitudes Atlantic surface water masses gain density due to increasing salinity (because of evaporation) and decreasing temperatures (cold winds from Canada and Greenland). Eventually they start to sink to intermediate water depths and even to the sea floor in distinct places such as the Greenland Sea, among others (Broecker & Denton 1989; Berger 1990; Broecker et al. 1990). According to the model, these oxygenated, cold and nutrient-depleted deep waters travel as far as into the North Pacific where they upwell, release salt, gain heat and return to the tropical Atlantic as the shallow branch of the Conveyor. Mainly surface waters from the south replace the quantum of water that is involved in the process of deep-water renewal, thus carrying heat to the north and providing a mild climate over northern Europe. Any disruption of this global ocean current circulation caused by processes such as changing salinity and temperature results in regional, hemispherical, and even global climate change, in particular when occurring in the Nordic seas (e.g. Boyle & Keigwin 1987; Broecker et al. 1988; Jansen & Veum 1990; Keigwin & Lehman 1994, Rahmstorf 1995; Broecker 1997; Ganopolski & Rahmstorf 2001).

It is of great importance for climate research to trace ocean currents and to know about the flow speed since the ocean currents are not only reacting to climate change, they are directly involved in shaping the impact of any change of the boundary conditions (e.g. Bond et al. 1992, 1993). Many studies focus on important aspects of the surface ocean (e.g. Bauch 1997; Chapman et al. 2000). Knowledge regarding the speed of

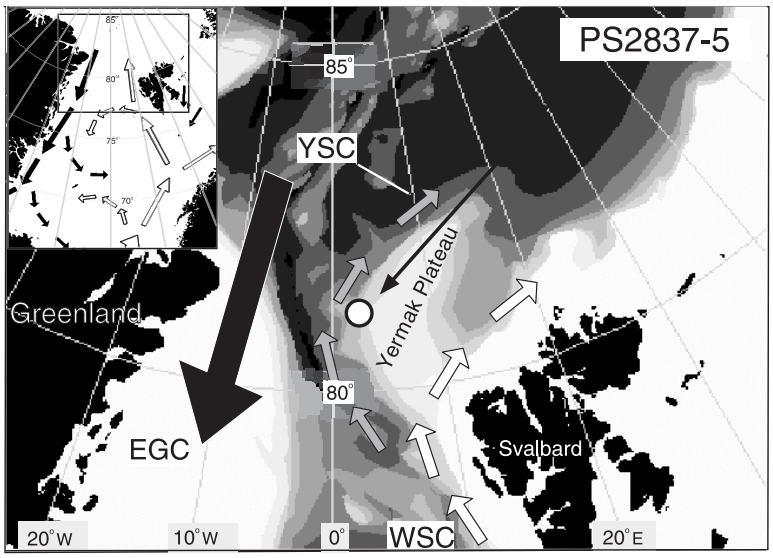

Fig. 1. Location of core PS2837-5, surface and subsurface (shaded = subsurface: Yermak Slope Current) currents (after Schlichtholz & Houssais 1999b). EGC = East Greenland Current (cold); WSC = West Spitsbergen Current (temperate). The white dot marks the position of core PS2837.

deep currents, however, is comparably sparse and usually restricted to areas of "suitable" sedimentation (e.g. Bianchi & McCave 2000; Hall & McCave 2000). Although ocean currents bearing important climate information also occur in the high latitudes, such as the Arctic Ocean, palaeocurrent speed reconstructions from these regions are very rare.

Grain size analysis is the most important way to learn about the speed of bottom currents in places where current transport is the only transport process. Every single terrigenous grain requires a certain current energy to be transported to the place the sample was taken if it was exclusively transported by currents. Sediments from high latitudes or glacial sediments, however, usually contain a certain amount of ice-rafted debris (IRD), which tends to corrupt the data base for current speed analyses. Although IRD released from icebergs and/or from sea ice is often in the sand fraction (or even coarser), it may also contain other grain sizes (Clark & Hanson 1983; Pfirman et al. 1989; Nürnberg et al. 1994). Hebbeln (2000), who found terrigenous material in sediment traps in Fram Strait well above the bottom nepheloid layer, related grain sizes >10 µm to IRD events. He proposed the fraction >40 µm to be the most promising tool to reconstruct palaeo sea ice extensions. However, bottom currents in Fram Strait may be able to transport grains >40 µm at times when current speed is between 10 and 15 cm/s, which would strongly bias either interpretation (see von Gyldenfeldt et al. 2000).

Thus, eliminating material of a certain grain size—a method that is often applied—in order to produce a sample that is suitable for current-speed related analyses, is not recommended. Misinterpretations regarding current strength may occur when IRD forms part of the silt or clay fractions. To address this common sedimentological problem, a new method to reduce influences of IRD on a sediment record from the Yermak Plateau is introduced in this study.

Current speed and sortable silt

The determination of palaeocurrent speed is usually based on information gained from grain size distributions of "suitable sediments" which combine a variety of frame conditions crucial for interpretations. These include a constant sediment source, constant direction of those (bottom) currents that sort the sediments, sortable sediments and no external processes such as input of IRD, turbidity currents or any other type of gravitational mass movement.

Sortable sediments include those grain size fractions that are physically sortable by the bottom currents under investigation. Since small grain diameters (clay to fine silt) tend to form aggregates that may not behave in an interpretable way, the "sortable silt fraction" (10-63 µm) has been suggested to be most

suitable for palaeocurrent speed reconstruction (McCave et al. 1995a, 1995b; Bianchi & McCave 1999). This fraction is non-cohesive and therefore well sortable by deep marine currents, and the grain size range can be related to the speed range of marine bottom currents in non-exceptional environments. Since short-term events may last only days, or even hours, they cannot usually be resolved in deep sea sediment samples. Thus, information gained from the sortable silt fraction represents information on mean current speed.

The sortable silt fraction is subject to relative changes related to changes in sediment supply like all other sediment compounds. The most suitable parameter to overcome these difficulties and to get best information on general granulometric trends is the sortable silt mean grain size ($\overline{SS}$) (McCave et al. 1995a). This parameter is largely independent from sediment supply. It depends exclusively on the strength of the bottom currents if all other frame conditions are fulfilled. $\overline{SS}$ provides a comprehensive characterization of the sample. It proved to be more suitable than other parameters such as graphic determinations of statistical parameters since it is calculated using all subfractions (about 27) instead of only a few percentiles.

Hydrography of the Fram Strait–Arctic Ocean gateway

Fram Strait forms the only deep oceanic gateway between the Arctic Ocean and the World Ocean. It is characterized by two contrasting surface currents: the West Spitsbergen Current (WSC) and the East Greenland Current (EGC) (Aagaard et al. 1987; Gascard et al. 1995). Atlantic surface water masses enter eastern Fram Strait and pass Svalbard as the WSC. This stream of temperate water masses bifurcates north of Svalbard as a result of the topography (Fig. 1). The upper ca. 500 m of the WSC is deflected to the east north of Svalbard due to Coriolis forcing. Due to the sill depth, water masses deeper than 500 m, such as the Yermak Slope Current (YSC; Fig. 1) are forced to flow along the western Yermak Plateau. A variety of water masses are identified in Fram Strait. Among them, northerly directed water masses, in particular Norwegian Sea Deep Water (NSDW) (ca. 1-3 km of water depth), and overlying mixed and modified primarily Atlantic-source water masses as well as a significant amount of ice originating from the south-directed Transpolar Drift, influence sedimentation at the core location (Schlichtholz & Houssais 1999a; Stein & Fahl 1997; Swift & Koltermann 1988). Inflow into the Arctic Ocean takes place via the eastern Fram Strait; outflow is primarily constrained to western Fram Strait, where the East Greenland Current carries Arctic water masses southward. Recirculation takes place in various areas between in- and outflow in the entire Fram Strait (Manley 1995). The core location is situated north of the modern summer ice margin primarily under the influence of north-directed NSDW (Fig. 1).

Materials and methods

The investigated sediment core (kastencore PS2837-5) was recovered from the western Yermak Plateau at 81° 13.99' N, 2° 22.85' E during the expedition ARK XIII/2 of RV *Polarstern* (Stein & Fahl 1997). The core location is on the slope shoulder at 1042 m water depth. In this methodological study, data from the upper 280 cm of the core are presented, covering the time period from the Bølling–Allerød warm phase to the Present.

The sediment core was sampled in slices of 1 cm thickness. After freeze-drying the samples were treated with hydrogen peroxide to remove organic matter. Wet-separation of the sand (>63 μm) was carried out using a standard sieve. The fraction <63 μm was collected in 500 ml plastic bottles. After the addition of sodium polyphosphate for better dispersion, the sample containers were put on a shaker for a minimum of 24 h. Analysis of the silt (in 0.1 phi steps) and clay was carried out using standard methods including a Sedigraph 5100 (Robinson & McCave 1994). All percentage values given in the text are weight percentages. Due to very low amounts, removal of carbonate and biogenic silica was not necessary.

Radiocarbon age determinations were carried out on five samples (approximately 2000 tests each) of the planktonic foraminifer *Neogloboquadrina pachyderma* (sinistral) (Spielhagen & Nørgaard-Pedersen unpubl. data). Measurements and laboratory work was carried out at the accelerator mass spectrometer facility at the Leibniz Laboratory, Kiel University. A reservoir correction of 400 years was applied. The reservoir-corrected data were converted to calendar years BP (Present = AD 1950) using CALIB 4.1.2 (see

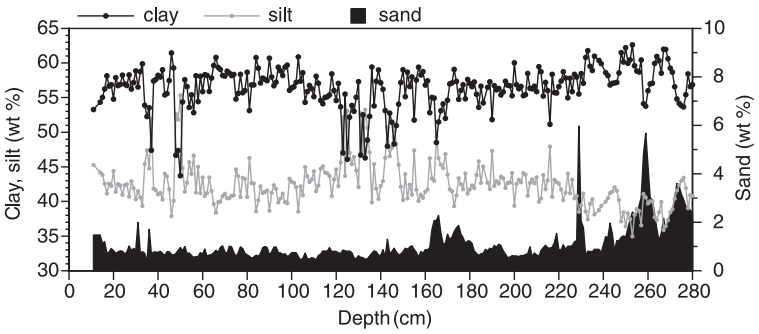

Fig. 2: Bulk sand, silt, and clay distributions of core PS2837-5.

Stuiver et al. 1998). In the following text all age data are given in calendar years BP.

Bulk grain size distributions

Through the entire core section presented here the sand content varies between 0.3 and 6%, silt ranges between 34 and 56%, and the clay content lies between 43 and 63% (Fig. 2). In the Holocene section of the core (from ca. 230 cm core depth) sand contents decrease to values between 0.2 and 2.5% and silt ranges between 38 and 56% (with a mean value of 43%). Clay contents are between 43 and 62%; the clay average is at 57%. Around 230 cm core depth sand and clay contents decrease whereas the silt content increases. Another change occurs at 130 cm core depth: silt decreases and clay increases, but the sand content does not show any clear trend other than slightly increased values between 180 and 160 cm.

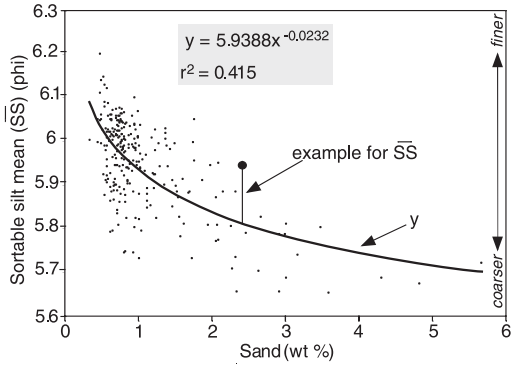

Fig. 3. Sand/$\overline{SS}$ relationship in core PS2837-5 (0-280 cm section) (see text).

Reducing the ice-rafted silt influence from the current-sorted silt fraction

Bottom currents are usually not strong enough to transport sand-sized material far along the western Yermak Plateau (see von Gyldenfeldt et al. 2000 for 79° N mooring data; Schauer pers. comm. 2000). There are no direct current speed measurements from the area. Generally, however, grain size compositions of the samples rule out regularly occurring current velocities that would be necessary to transport sand-sized material. Thus, the sand fraction is assumed to be largely if not entirely ice-rafted.

If the sand-sized material is predominantly ice-rafted and the silt fraction is primarily current-sorted then there should be no direct correlation between the sand and silt fractions. This assumption is supported by the fact that IRD deposition increases during cold (glacial and deglacial) periods (e.g. Hebbeln & Wefer 1997; Hald et al. 2001; unpublished data from the core presented here), whereas the speed of those deep currents fed by deep-water production usually decreases during cold periods (e.g. Manighetti & McCave 1995; Bianchi & McCave 1999). Thus, there are processes that largely prevent massive occurrence of IRD and current speed high enough to transport sand within the same time interval.

Figure 3 shows that the correlation between sand (wt %) and $\overline{SS}$ is $r^2 = 0.41$. The relation is similar when calculated with sand accumulation rate data ($g*cm^{-2}*Ky^{-1}$). Though weak, the correlation suggests a similar mode of transportation of sand and silt where data points plot close to the function (y). Since current transport of the sand can largely be ruled out, it is suggested that part of the silt fraction is ice-rafted. The correlation

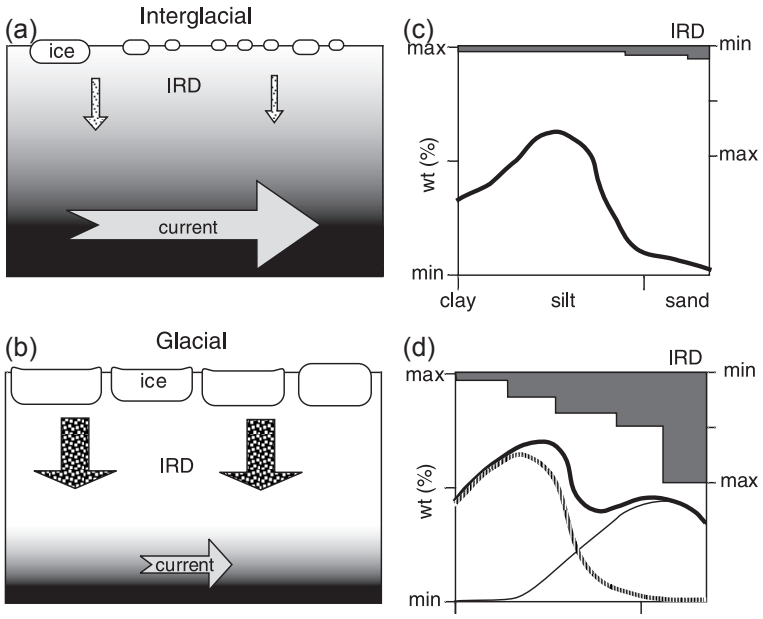

Fig. 4. Sketch of potential conditions during cold and warm climate phases: (a) increased current speed but decreased IRD flux during a potential interglacial; (b) increased IRD flux but lower current speed during a potential glacial. (c) Potential grain size frequency curve during a warm phase (low IRD flux marked on top); (d) potential grain size frequency curve during a cold phase (high IRD flux marked on top). The thick solid lines mark the frequency curves as they would be measured (IRD contaminated). In (d) the broken line marks the potential current-sorted fraction; the thin solid line marks the potential IRD fraction.

is positive, meaning that increasing sand content causes the silt fraction to coarsen. Thus, it is most plausible that part of the silt is ice-rafted, behaving like the coarser IRD. Fig. 4 (as a model example) shows that the sand mode most likely extends to the silt fraction, thereby contaminating the coarser part of this fraction. The regression equation for the core section presented in this study is as follows:

$$y = 5.9388\ x^{-0.0232} \quad (1)$$

with y = sortable silt mean size ($\overline{SS}$) of sediment primarily influenced by ice rafting and x = sand content in wt %.

The regression function y describes the correlation between the two parameters. This curve represents "average" relations between silt grain size and IRD. Samples that plot on the curve show a correlation coefficient of $r^2 = 1$; these were deposited during times of "average" conditions. Accordingly, samples that show deviations from the regression line were deposited under changed frame conditions. These may include a certain variation in the IRD composition at the time the sample was deposited or/and variation in current speed. Changes in IRD composition can never be ruled out. There are no means, though, that would permit the determination of the exact amount of ice-rafted silt. However, the process of incorporation of terrigenous material in ice, as well as the process of release of ice-rafted material from ice, is a random process. It is not likely that random processes result in steady changes in the composition of associated sediments. Thus, if steady changes occur it is most likely that fluctuations in bottom current speed had triggered them.

The regression function y allows the potential $\overline{SS}$ ($\overline{SS}_{pot}$) to be calculated by inserting the sand values into the function. The resulting record $\overline{SS}_{pot}$ describes how the $\overline{SS}$ distribution would have been if there were no current-speed fluctuations (Fig. 5c). Subtracting $\overline{SS}_{pot}$ from the measured $\overline{SS}$ yields deviations from $\overline{SS}_{pot}$ (deviation in the coarse or in the fine direction) (Eq. 2; see also Fig. 3). Coarser than $\overline{SS}_{pot}$ (i.e. coarser than y in Fig. 3) means that bottom currents must have been stronger to provide higher transport energy; finer than $\overline{SS}_{pot}$ (i.e. finer than y in Fig. 3) means that the sample was indeed finer than the calculated value, thus bottom currents must have been slower to produce this sediment. Hence, the IRD-corrected parameter can be interpreted in terms of relative current-speed fluctuations; it is called $\Delta\overline{SS}$.

$$\Delta\overline{SS} = \overline{SS} - \overline{SS}_{pot} \quad (2)$$

with $\Delta\overline{SS} = \overline{SS}$ component that is modulated by current speed, $\overline{SS}$ = sortable silt mean size as measured and $\overline{SS}_{pot} = \overline{SS}$ of sediment primarily influenced by ice rafting (equals y in Eq. 1).

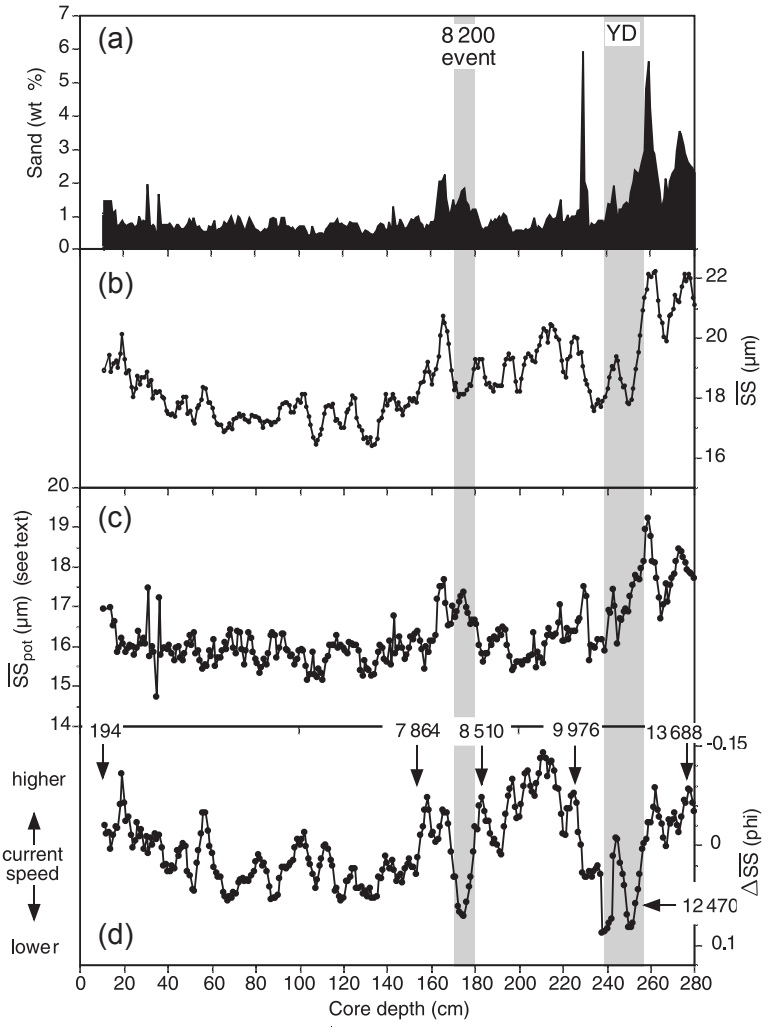

Fig. 5. Transformation of the silt mean grain size curve (see text): (a) sand; (b) sortable silt mean grain size as measured; (c) $\overline{SS}_{pot}$ (calculated, see text); (d) current-sorted fraction of the sortable silt mean grain size ($\Delta\overline{SS}$). Numbers and arrows mark calendar years BP. Panels (b) and (c) are given in µm rather than phi for better understanding. Panels (b) and (d) are unweighted 5 pt. running means.

Figure 5 shows the transformation from the uncorrected to the corrected silt curve related to the sand curve that forms the basis of the calculations. The correction usually sharpens peaks and makes the curve more pronounced by reducing the influence of ice-rafted material.

Preliminary interpretation of the current speed record

Here the results of the methodological approach are briefly discussed. Comprehensive interpretations of climate-steered oceanographic changes will be published elsewhere (Hass et al. in prep.). Figure 5 reveals the parameters that form part of the equations. The sand content decreases towards the Holocene, with some stronger fluctuation during the termination phase (ca. 280 - 230 cm core depth; Fig. 5a). The $\overline{SS}$ curve appears basically to resemble the sand curve, although there seems to be no linear relation (Fig. 5b). Figure 5c reveals $\overline{SS}_{pot}$ that shows $\overline{SS}$ under abstraction of current speed caused fluctuations (i.e. the part that shows predominantly the influence of ice rafting calculated from Eq. 1). This curve naturally resembles the sand curve since the sand fraction is interpreted to be nearly exclusively composed of IRD. Fig. 5d shows the current speed modulated portion of curve 5b. Since this curve is interpreted to be principally influenced by currents of the YSC, which is primarily composed of NSDW produced in the Greenland Sea, it is also supposed to reflect the

strength of deep-water formation to a certain degree aside from current speed. A variety of investigations suggest that deep-water formation was at least reduced during the glacials and strong during the interglacials (e.g. Broecker & Denton 1989; Maslin et al. 1995). The same may be true for cold and warm climate fluctuations within these climate phases (see Bianchi & McCave 1999; Austin & Kroon 2001).

With regard to relative palaeocurrent speed analyses, the $\overline{SS}$ and the IRD-corrected $\Delta\overline{SS}$ curves are principally not too different. However, when directly compared, there are some notable differences. Prior to the Younger Dryas cold phase (280 - 260 cm core depth) the $\overline{SS}$ curve shows the highest values in the record, whereas the $\Delta\overline{SS}$ curve suggests highest current speed between 230 and 155 cm core depth. It becomes evident that high $\overline{SS}$ values during the Bølling–Allerød warm phase are obviously the result of ice-rafted silt biasing the record. In the IRD-corrected curve, strongest currents are suggested during the early Holocene, likely marking climate optimum conditions. Lowest $\overline{SS}$ values occur during the mid Holocene (60 - 150 cm core depth). Much better fitting to the climate record, $\Delta\overline{SS}$ suggests that the lowest current speed of the past 13 700 years occurred exactly during the Younger Dryas and the 8200 year event cold phases. There is consensus that these two phases were the coldest and most prominent of the time period observed here (Alley et al. 1997; Alley 2000). Moreover, both periods are described to have been accompanied by a reduction in deep-water formation (Broecker & Denton 1989; Barber et al. 1999). This was obviously the case in those places where the water mass originates that feeds the YSC. According to the record presented here, current speed during the mid Holocene was comparably low. Whether or not this mirrors the strength of thermohaline overturn in the Nordic seas during the mid Holocene has yet to be investigated. The youngest part of the Holocene appears in both records as a period of increasing current speed. Similarly, it can only be speculated that this might be a reaction to increasing thermohaline overturn in the Nordic seas.

Summary and conclusion

This study presents a new approach to reduce the influence of silt-sized ice-rafted material from silt-sized current-sorted sediment. The method is based on the assumption that sand-sized material was almost exclusively ice-rafted. Thus, the grade of resemblance between silt and sand can be used to calculate relative bottom current velocities. Application of this method to a sediment core from the Yermak Plateau yields improvement of the clarity of the sortable silt mean grain size ($\overline{SS}$) record that is transformed into the parameter $\Delta\overline{SS}$ (introduced in this study), the current speed controlled portion of $\overline{SS}$. Climate phases such as the Holocene Optimum (here between 9900 and 8500 years BP), the Younger Dryas, and even the 8200 cold event occur with suggestive significance. The latter cold phase is not significant in the original record. Although the method introduced in this paper yields promising results, it can only be applied to other areas which fulfill a number of frame conditions.

Acknowledgements.—I thank I. N. McCave, G. Bianchi, D. K. Fütterer, R. Stein and J. Matthiessen for comments on an earlier draft of this paper. Review by R. Spielhagen and an anonymous reviewer are much appreciated. P. Grootes and H. Erlenkeuser are thanked for valuable discussions.

References

Aagaard, K. A., Foldvik, S. R. & Hillman, S. R. 1987: The West Spitsbergen Current: deposition and watermass transformation. *J. Geophys. Res. 92(C4)*, 3778–3784.

Alley, R. 2000: The Younger Dryas cold interval as viewed from central Greenland. *Quat. Sci. Rev. 19*, 213–226.

Alley, R., Mayewski, P. A., Sowers, T., Stuiver, M., Taylor, K. C. & Clark, P. U. 1997: Holocene climate instability: a prominent wide-spread event 8200 y ago. *Geology 25*, 483–486.

Austin, W. E. N. & Kroon, D. 2001: Deep sea ventilation in the northeastern Atlantic during the last 15,000 years. *Glob. Planet. Change 30*, 13–31.

Barber, D. C., Dyke, A., Hillaire-Marcel, C., Jennings, A. E., Andrews, J. T., Kerwin, M. W., Bilodeau, G., McNeely, R., Southon, J., Morehead, M. D. & Gagnon, J.-M. 1999: Forcing of the cold event of 8,200 years ago by catastrophic drainage of Laurentide lakes. *Nature 400*, 344–348.

Bauch, H. A. 1997: Paleoceanography of the North Atlantic Ocean during the past 450 ky deduced from planktic foraminiferal assemblages and stable isotopes. In H. C. Hass & M. A. Kaminski (eds.): *Contributions to the micropaleontology and paleoceanography of the northern North Atlantic. Grzybowski Found. Spec. Publ. 5.* Pp. 83–100. Krakow.

Berger, W. H. 1990: The Younger Dryas cold spell—a quest for causes. *Palaeogeogr. Palaeoclimatol. Palaeoecol. 89*,

219–237.
Bianchi, G. & McCave, I. N. 1999: Holocene periodicity in North Atlantic climate and deep-ocean flow south of Iceland. *Nature 397*, 515–517.
Bianchi, G. G. & McCave, I. N. 2000: Hydrography and sedimentation under the deep western boundary current on Björn and Gardar drifts, Iceland Basin. *Mar. Geol. 165*, 137–169.
Bond, G., Broecker, W. S., McManus, J., Labeyrie, L., Louzel, J. & Bonani, G. 1993: Correlations between climate records from North Atlantic sediments and Greenland ice. *Nature 365*, 143–147.
Bond, G., Heinrich, H., Huon, S., Broecker, W. S., Labeyrie, L., Andrews, J., McManus, J., Clasen, S., Tedesco, K., Jantschik, R., Simet, C. & Klas, M. 1992: Evidence for massive discharge of icebergs into the glacial North Atlantic. *Nature 360*, 245–249.
Boyle, E. A. & Keigwin, L. 1987: North Atlantic thermohaline circulation during the past 20,000 years linked to high-latitude surface temperature. *Nature 330*, 35–40.
Broecker, W. S. 1991: The great ocean conveyor. *Oceanography 4*, 79–89.
Broecker, W. S. 1997: Thermohaline circulation, the Achilles heel of our climate system: will man-made CO_2 upset the current balance? *Science 278*, 1582–1588.
Broecker, W. S., Andree, M., Wolfli, W., Oeschger, H., Bonani, G., Kennett, J. & Peteet, D. 1988: The chronology of the last deglaciation: implications to the cause of the Younger Dryas event. *Paleoceanography 3*, 1–19.
Broecker, W. S., Bond, G. & Klas, M. 1990: A salt oscillator in the glacial Atlantic: 1. The concept. *Paleoceanography 5*, 469–477.
Broecker, W. S. & Denton, G. H. 1989: The role of ocean-atmosphere reorganizations in glacial cycles. *Geochim. Cosmochim. Acta 53*, 2465–2501.
Chapman, M. R., Shackleton, N. J. & Duplessy, J.-C. 2000: Sea surface temperature variability during the last glacial–interglacial cycle: assessing the magnitude and pattern of climate change in the North Atlantic. *Palaeogeogr. Palaeoclimatol. Palaeoecol. 157*, 1–25.
Clark, D. L. & Hanson, A. 1983: Central Arctic Ocean sediment texture: a key to ice transport mechanisms. In B. F. Molnia (ed.): *Glacial marine sedimentation*. Pp. 301–330. New York: Plenum.
Ganopolski, A. & Rahmstorf, S. 2001: Rapid changes of glacial climate simulated in a coupled climate model. *Nature 409*, 153–158.
Gascard, J. C., Richez, C. & Rouault, C. 1995: New insights on large-scale oceanography in Fram Strait: the west Spitsbergen Current. In W. Smith & J. Grebmeier (eds.): *Oceanography of the Arctic Ocean: marginal ice zones and continental shelves*. Pp. 131–182. Washington, D.C.: American Geophysical Union.
Hald, M., Dokken, T. & Mikalsen, G. 2001: Abrupt climate change during last interglacial-glacial cycle in the polar North Atlantic. *Mar. Geol. 176*, 121–137.
Hall, I. R. & McCave, I. N. 2000: Palaeocurrent reconstruction, sediment and thorium focussing on the Iberian margin over the last 140 ka. *Earth Planet. Sci. Lett. 178*, 151–164.
Hebbeln, D. 2000: Flux of ice-rafted detritus from sea ice in the Fram Strait. *Deep-Sea Res. II 42*, 1723–1790.
Hebbeln, D. & Wefer, G. 1997: Late Quaternary oceanography of the Fram Strait. *Paleoceanography 12*, 65–78.
Jansen, E. & Veum, T. 1990: Evidence for two-step deglaciation and its impact on North Atlantic deep water circulation. *Nature 343*, 612–616.
Keigwin, L. D. & Lehman, S. J. 1994: Deep circulation change linked to Heinrich event 1 and Younger Dryas in a middepth North Atlantic core. *Paleoceanography 9*, 185–194.
Manighetti, B. & McCave, I. N. 1995: Late glacial and Holocene paleocurrents around Rockall Bank, NE Atlantic Ocean. *Paleoceanography 10*, 611–626.
Manley, T. O. 1995: Branching of Atlantic water within the Greenland–Spitsbergen passage: an estimate of recirculation. *J. Geophys. Res. 100(C10)*, 20 627–20 634.
Maslin, M. A., Shackleton, N. J. & Pflaumann, U. 1995: Surface water temperature, salinity, and density changes in the northeast Atlantic during the last 45,000 years: Heinrich events, deep water formation, and climatic rebounds. *Paleoceanography 10*, 527–544.
McCave, I. N., Manighetti, B. & Beveridge, N. A. S. 1995a: Circulation in the glacial North Atlantic inferred from grain-size measurements. *Nature 374*, 149–152.
McCave, I. N., Manighetti, B. & Robinson, S. G. 1995b: Sortable silt and fine sediment size/composition slicing: parameters for palaeocurrent speed and palaeoceanography. *Paleoceanography 10*, 593–610.
Nürnberg, D., Wollenburg, I., Dethleff, D., Eicken, H., Letzig, T., Reimnitz, E. & Thiede, J. 1994: Sediments in Arctic sea ice: implications for entrainment, transport and release. *Mar. Geol. 119*, 185–214.
Pfirman, S., Wollenburg, I., Thiede, J. & Lange, M. A. 1989: Lithogenic sediment on Arctic pack ice: potential aeolian flux and contributions to deep sea sediments. In M. Sarnthein & M. Leinen (eds.): *Paleoclimatology and paleometeorology: modern and past patterns of global atmospheric transport*. Pp. 463–493. Dordrecht: Kluwer.
Rahmstorf, S. 1995: Bifurcations of the Atlantic thermohaline circulation in response to changes in the hydrological cycle. *Nature 378*, 145–149.
Robinson, S. G. & McCave, I. N. 1994: Orbital forcing of bottom-current enhanced sedimentation on Feni Drift, NE Atlantic, during the mid-Pleistocene. *Paleoceanography 9*, 943–972.
Schlichtholz, P. & Houssais, M.-N. 1999a: An inverse modeling study in Fram Strait. Part I: dynamics and circulation. *Deep-Sea Res. II 46*, 1083–1135.
Schlichtholz, P. & Houssais, M.-N. 1999b: An inverse modeling study in Fram Strait. Part II: water mass distribution and transports. *Deep-Sea Res. II 46*, 1137–1168.
Stein, R. & Fahl, K. 1997: *Scientific cruise report of the Arctic Expedition ARK XIII/2 of RV "Polarstern" in 1997. Ber. Polarforsch. 255*.
Stuiver, M., Reimer, P. J., Bard, E., Beck, J. W., Burr, G. S., Hughen, K. A., Kromer, B., McCormac, G., van der Pflicht, J. & Spurk, M. 1998: INTCAL 98 Radiocarbon age calibration, 24,000-0 cal BP. *Radiocarbon 40*, 1041–1083.
Swift, J. H. & Koltermann, K. P. 1988: The origin of Norwegian Sea deep water. *J. Geophys. Res. 93(C4)*, 3563–3569.
von Gyldenfeldt, A., Carstens, J. & Meincke, J. 2000: Estimation of the catchment area of a sediment trap by means of current meters and foraminiferal tests. *Deep-Sea Res. II 47*, 1701–1717.